ASME Journal of Solar Energy Engineering
Online journal at:
https://asmedigitalcollection.asme.org/solarenergyengineering

Katherine Bassett
Department of Civil and Environmental Engineering,
Northeastern University,
360 Huntington Avenue,
Boston, MA 02115

Rachel Silcox
Department of Mechanical Engineering,
University of Michigan,
2350 Hayward,
Ann Arbor, MI 48109

Jeffrey D. Will
Department of Electrical Engineering,
Valparaiso University,
Valparaiso, IN 46383

Sarah Hill
Department of Chemistry,
Valparaiso University,
Valparaiso, IN 46383

Paul Smith
Department of Chemistry,
Valparaiso University,
Valparaiso, IN 46383

Ben Smith
Department of Mechanical Engineering,
Valparaiso University,
1900 Chapel Drive,
Valparaiso, IN 46383

Brian Schmit
Department of Mechanical Engineering,
Valparaiso University,
1900 Chapel Drive,
Valparaiso, IN 46383

Luke J. Venstrom
Department of Mechanical Engineering,
Valparaiso University,
1900 Chapel Drive,
Valparaiso, IN 46383

Fungible, Multiyear Solar Thermochemical Energy Storage Demonstrated via the Cobalt Oxide Cycle[1]

We present a proof of concept demonstration of solar thermochemical energy storage on a multiple year time scale. The storage is fungible and can take the form of process heat or hydrogen. We designed and fabricated a 4-kW solar rotary drum reactor to carry out the solar-driven charging step of solar thermochemical storage via metal oxide reduction–oxidation cycles. During the summer of 2019, the solar reactor was operated in the Valparaiso University solar furnace to effect the reduction of submillimeter cobalt oxide particles in air at approximately 1000°C. A particle collection system cooled the reduced particles rapidly enough to maintain conversions of 84–94% for feed rates of $2.9 - 60.8\ g\ min^{-1}$. The solar-to-chemical storage efficiency, defined as the enthalpy of the reduction reaction at 1000°C divided by the solar energy input, reached 20%. Samples of the reduced cobalt oxide particles were stored in vials in air at room temperature for more than 3 years. The stored solar energy was released by reoxidizing samples in air in a benchtop reactor and by electrochemically reoxidizing samples to produce H_2. Measurements of the oxygen uptake by the reduced metal oxide confirm its promise as a medium to store and dispatch solar energy over long durations. Linear sweep voltammetry and bulk electrolysis demonstrate the promise of H_2 production at 0.55 V relative to the normal hydrogen electrode, 0.68 V below the 1.23 V potential required for conventional electrolysis.
[DOI: 10.1115/1.4065102]

Keywords: thermochemical energy storage, solar reactor, cobalt oxide, hydrogen, solar, testing

[1]Portions of this article were published in the Proceedings of the 2023 ASME Energy Sustainability Conference.
[2]Corresponding author.
Contributed by the Solar Energy Division of ASME for publication in the Journal of Solar Energy Engineering: Including Wind Energy and Building Energy Conservation. Manuscript received September 29, 2023; final manuscript received January 31, 2024; published online April 23, 2024. Assoc. Editor: Julia Haltiwanger Nicodemus.

Peter T. Krenzke[2]
Department of Mechanical Engineering,
Valparaiso University,
1900 Chapel Drive,
Valparaiso, IN 46383

1 Introduction

With increasing adoption of sustainable but intermittent energy sources, the need for energy storage is growing. The solar resource is especially abundant, making means to store its energy in stable, dispatchable forms particularly desirable. Among solar energy storage approaches, solar thermochemical pathways are of interest because they produce chemical products with high-energy density that can be stored for hours, days, or even years.

In this work, we demonstrate a multiyear thermochemical energy storage approach using a metal oxide energy carrier. Energy from concentrated sunlight is stored through the reduction of cobalt oxide particles, Eq. (1), which we refer to as the charging step. Later the stored solar energy is released either through the oxidation of the reduced particles by gaseous oxygen, Eq. (2), or through the electrochemical oxidation of the particles by water in an aqueous electrolyte to produce H_2, Eq. (3).

$$Co_3O_4 \rightarrow 3CoO + 1/2O_2 \tag{1}$$

$$3CoO + 1/2O_2 \rightarrow Co_3O_4 \tag{2}$$

$$3CoO + H_2O \rightarrow Co_3O_4 + H_2 \tag{3}$$

Cobalt oxide is chosen as the energy carrier in this work because it has several advantageous characteristics. Similar to other metal oxides, the reduction reaction (Eq. (1)) requires elevated temperatures. In this case, the temperature is near 1000°C, for which central tower receiver systems are well suited to provide solar process heat. Cobalt oxide may be reduced in air at this temperature, avoiding the energetic and capital equipment costs of operating with low oxygen concentrations required by many other candidate metal oxide energy carriers. Reducing the metal oxide in air also allows the possibility to implement the solar-driven reduction in windowless receiver-reactors. Compared to other oxides reducible in air at these temperatures, cobalt oxide has warranted attention as a storage medium because of the high heat of reaction, $\Delta H_r = 844\,\mathrm{kJ/kg{-}Co_3O_4}$ [1–3]. The reduced CoO can be stored indefinitely in room temperature air, making cobalt oxide an especially attractive candidate for solar energy storage over long durations.

While both thermodynamic and certain practical characteristics of energy storage with cobalt oxide are promising, we acknowledge that its toxicity adds an important constraint to its implementation. Especially hazardous to aquatic life, any industrial implementation must ensure that the cobalt oxide is fully retained in a controlled system. Cobalt oxide is also carcinogenic, requiring special care to prevent inhalation when working with particles. In addition to concerns about cobalt oxide's toxicity, Buck et al. rightfully draw attention to anthropological concerns about its sourcing [4]. Still we find its technical characteristics warrant continued evaluation, as it holds promise both for solar thermal decoupled electrolysis [5] and thermochemical energy storage for high-temperature power cycles [6].

There are two relevant strategies for releasing the energy stored in the reduced cobalt oxide. First, the energy may be released as process heat, for example, by reacting the reduced cobalt oxide (CoO) with a flow of air at elevated temperatures. The energy released by the oxidation of the CoO is transferred to the air as sensible heat. This strategy is amenable to supplying process heat to a high-temperature, high-efficiency power cycle [6–13]. Anticipated thermal efficiencies exceed 50% for supercritical CO_2 Brayton cycles operating with turbine inlet temperatures over 700 °C [14,15]. We note that cobalt structures have been studied as the storage medium for this energy release strategy by several research groups [6–9,12,13,16]. For the charging step, cobalt oxide structures can be reduced under a flow of compressed air, which has been heated to temperatures near 950 °C in a solar receiver.

In the second energy release strategy, reduced cobalt oxide particles are supplied to an electrochemical cell to reduce the electrical work required to produce hydrogen with near room temperature water electrolysis. This latter approach was introduced by Palumbo et al. as the solar thermal decoupled electrolysis process [5,17,18]. A key feature of solar thermal decoupled electrolysis is that the solar-driven reduction and nonsolar electrochemical hydrogen production steps are decoupled in space and time. The cobalt oxide energy carrier has several characteristics, which facilitate the hydrogen-producing electrolysis step. The solar-produced CoO is readily dissolved in an electrolyte, and the solid product CoOOH (from which heating in air recovers Co_3O_4) precipitates from the solution [17]. Recently, the potential obstacle of anode passivation was addressed as we demonstrated the cobalt oxide product formed during hydrogen production is electrochemically active [18]. The most significant electrochemistry challenge is increasing the current density, though the use of high surface area porous electrodes is suggested as a potential solution [17], and the inducing flow in the electrochemical cell shows some promise [18].

In this work, we investigate reduction of cobalt oxide particles, which may be paired with either energy release strategy. We also evaluate the capacity of the reduced cobalt oxide particles to supply the stored energy on demand, both by releasing the stored energy as process heat through reaction with air and by producing H_2 with an electrical work input lower than that for conventional electrolysis. We choose to work with cobalt oxide in the particle form because they can serve both as the medium for thermochemical storage and as the solar receiver heat transfer "fluid." Particle receivers are one of the three types selected for the development by NREL in the Gen3 concentrated solar power roadmap, the other two being advanced molten salts and high pressure gases. Advantages of the particle pathway include high-energy storage density, scalability, an ability to operate receivers at relatively higher fluxes, and relatively lower parasitic energy requirements [19].

The solar reduction of cobalt oxide particles has been studied previously. Notably, at the DLR, Neises et al. demonstrated the reduction of Co_3O_4 to CoO in a windowed rotary kiln reactor in batch operation [1]. A controlled flow of air was employed both as the oxidizer gas and as a sweep gas to remove oxygen evolved during reduction. The average conversion of Co_3O_4 to CoO was 40–50% with a maximum conversion of 70% for a single batch. Neises et al. recommended the development of a continuously fed particle reactor with improved mixing as important advancements.

Rotary solar reactor-receivers are attractive for working with particles because of the high degree of mixing, which can aid mass and heat transport. Prior applications of rotary reactor-receivers include rotary kilns for the calcination of $CaCO_3$ to produce lime [20,21] and a conical rotary receiver for the thermal decomposition of ZnO [22]. Rotary particle receivers also lend themselves to scale up. A 2.5 MW rotary receiver has been designed and tested with receiver temperatures as high as 965 °C [23,24]. Continuously fed

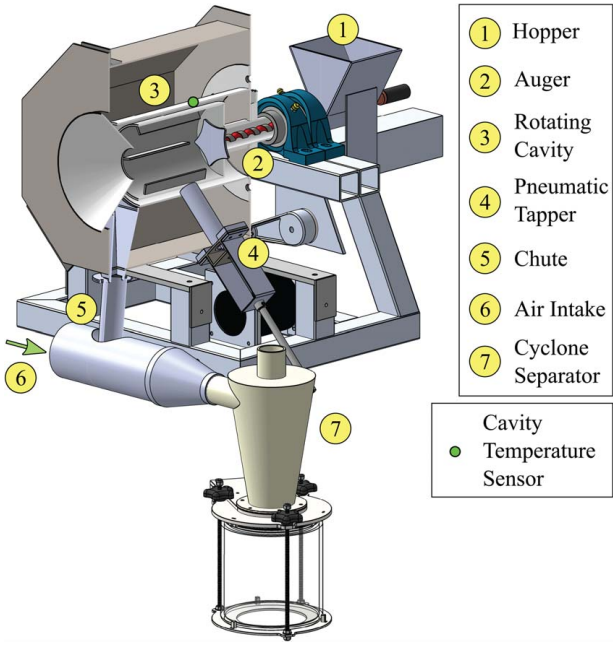

Fig. 1 The rotary drum reactor

particle reactors have been modeled by Tescari et al. at DLR [21] and by Kopping et al. at Valparaiso University [25]. Importantly Kopping et al. showed that the reactor performance is insensitive to both the particle volume fraction and the degree of axial mixing in the reactor. Further, it was concluded that the feed rate of cobalt oxide particles could be adjusted to maximize efficiency [25]. Palumbo et al. describe the development and the initial testing of a rotary drum reactor at Valparaiso University [26]. The initial testing evaluated feed rates of $4-30\,\mathrm{g\ \ min^{-1}}$ with demonstrated conversion as high as 84.8%. From the results, it was inferred that the cavity temperature must be maintained above 950 °C to facilitate high conversion.

In this work, we present a complete demonstration of solar thermochemical energy charging, storage, and release using cobalt oxide particles. The demonstration is composed of a new set of on-sun experiments where cobalt oxide particles were reduced in the 4 kW solar thermal rotary drum reactor developed at Valparaiso University with an improved feed system, the physical storage of the reduced particles for more than 3 years, and finally the on-demand release of the stored energy as process heat or H_2 in off-sun benchtop reactors. Based on the prior modeling and experimental assessment of the solar rotary drum reactor, the on-sun experimental program focuses on increasing the feed rate and conversion of the cobalt oxide particles [25,26]. In the following sections, we describe the salient solar reactor features and our experimental program, which demonstrates the viability of the concept.

2 The Rotary Drum Reactor

A windowless rotary drum reactor, shown in Fig. 1, was designed to effect the continuous solar-driven reduction of cobalt oxide particles in air at temperatures near 1000 °C [26]. Concentrated sunlight enters the reactor through a 6 cm windowless aperture. The reactor features an auger-driven feeding system and a rotating Inconel 625 cavity, 21.6 cm long with 13.5 cm diameter, that generates a particle cloud for volumetric absorption.

Cobalt oxide (Co_3O_4) particles are stored in a stainless steel hopper ① and fed continuously through a stainless steel tube into the reactor by a steel auger ②. For clarity, circled numbers refer to the component locations and key in Fig. 1. A vibrator motor and stirrer mounted to the top of the hopper encourage continuous particle supply to the auger, while a stepper motor controls the speed of the auger to adjust the mass flowrate of cobalt oxide into the reactor. Particles enter the reactor cavity ③ through an opening in the center of the back wall, i.e., furthest from the aperture, and drop to the lower cavity wall. To prevent sintering as the particles enter the reactor, a star-shaped Inconel plate shields the opening from direct exposure to concentrated sunlight. Once in the cavity, concentrated sunlight directly irradiates the suspended cobalt particles providing the process heat to facilitate their reduction.

The cavity rotates on a cantilevered tube supported by two pillow-block graphite bearings at the back of the reactor. A chain-drive rotates the internal cavity at a mean rate of 53 rpm to generate a particle cloud. For comparison, the rotary kiln demonstrated by Neises et al. operated at a maximum of 6 rpm [1], while the rotary drum CentRec receiver was operated at approximately 45 rpm [24]. Paddles welded to the inner surface of the rotating cavity aid mixing of the particle suspension. To reduce accumulation of particles on the cavity walls, a pneumatically driven piston ④ strikes the cavity once every 30 s. Rotation is temporarily halted during the piston strike. To encourage particle motion from back to front, the reactor is positioned with a 9 deg downward inclination.

The collection system consists of a blower, cyclone separator, and connecting ductwork. The blower is positioned downstream of the separator and ductwork to provide a favorable pressure gradient that pulls particles into the collection system from the cavity. Particles enter the collection system at the bottom front of the reactor through a chute ⑤. A camera mounted at the air intake ⑥ allows visual confirmation that particles are entering the collection system. The particles fall into a stainless steel collection tube and are cooled quickly with room temperature air drawn into the ductwork by the blower. Some larger particles accumulate in a tray positioned in the ductwork at the bottom of the collection tube. Smaller particles are captured in a glass jar by the cyclone separator ⑦. Downstream of the cyclone separator the air is filtered before exiting the blower.

3 Methods

3.1 On-Sun Solar Reduction. A series of on-sun experiments were conducted between July 11, 2019, and Aug. 7, 2019, to determine the impact of the particle feed rate on the cobalt oxide conversion and thermal efficiency during the charging step of the cycle. On-sun testing was carried out at the solar furnace housed in the James S. Markiewicz Solar Energy Research Facility at the Valparaiso University [27]. The solar furnace employs a horizontal, on-axis optical configuration in which a heliostat reflects solar radiation into a faceted, spherical concentrator. The concentrator is composed of 305 hexagonal shaped mirrors, has a focal length of 5.77 m, and a rim angle of approximately 20 deg. The concentrator focuses the radiation to an approximately 6-cm-diameter focal spot to which the solar reactor aperture was matched.

To produce Co_3O_4 used in the solar reactor experiments, Alfa Aesar 400 mesh $Co(OH)_2$ with particle sizes nominally less than 37 μm was heated in air at 750 °C for 12–24 h. Within measurement uncertainty, X-ray diffraction (XRD) confirmed 100% conversion to Co_3O_4 after the heat treatment, with no measurable difference between 12- and 24-h heating periods.

For each on-sun experiment, Co_3O_4 is loaded into the hopper at room temperature outside the reactor. Mostly fresh Co_3O_4 was used. However, some particles were retained in the hopper and the auger feed system from prior experiments. The reactor cavity is empty before the experiment. Just before placing the reactor on sun, the solar input power is measured with a CCD camera and water-cooled Lambertian target, which was calibrated against a calorimeter [28]. Once on-sun, the heat up period is usually 1–2 h, depending on the solar resource, i.e., direct normal irradiance (DNI), for the day. The reactor cavity temperature is measured

by a K-type thermocouple, positioned axially 21.7 cm from the aperture and 5.7 cm from the back wall of the rotating cavity. Radially, the thermocouple lies 8.4 cm from the cavity centerline, between the rotating cavity and 10 cm of insulation, such that we expect it to be close to the cavity wall temperature and slightly lower than the particle temperature. Once the cavity reaches its target temperature of approximately 1000 °C, the cavity rotation, piston, cooling system, hopper vibration motor, hopper stirrer, and feed auger are activated. Co_3O_4 is fed into the back of the cavity at a constant feed rate for a duration of 2–13 min at feed rates between 2.9 and 60.8 g min^{-1}. To stop feeding, the feed auger, hopper vibration motor, and hopper mixer are shut off while all other components are left on until material has stopped exiting the cavity. Once feeding has completely stopped, the reactor is taken off sun by closing the louvers at the entrance to the solar furnace.

Longer feeding durations, 20–30 min, were accomplished in earlier experiments in the reactor as described by Palumbo et al. [26]. We targeted shorter durations to limit the total amount of cobalt used in our experiments. The exact duration was set during operation of each experiment with the primary goal of maintaining the cavity temperature above 960 °C, for which the model developed by Kopping et al. predicts complete conversion [25]. Prior experiments with the solar rotary drum reactor resulted in low conversions, <50%, for temperatures below 950 °C, but higher conversions for 69–85% for operation above 1000 °C [26].

After each on-sun test, a total of 30–300 g of product material was collected separately from the tray just below the chute in the exhaust duct, the jar at the base of the cyclone separator, and the receiver cavity. Samples from the products collected at each location were characterized by X-ray diffraction (Rigaku Miniflex 600) to determine the composition of the sample within ±5% via Rietveld refinement of the resulting spectra.

For each experiment, the reactor efficiency was calculated according to Eq. (4)

$$\eta = \frac{m\,\bar{X}\,\Delta H_r}{\dot{Q}_{solar}\,t} \tag{4}$$

where m is the sum of masses collected from the tray at the base of the chute and the cyclone separator jar and $\bar{X}$ is the mass weighted average conversion of cobalt collected from the same locations. The mass weighted average conversion is calculated according to Eq. (5)

$$\bar{X} = \frac{\sum_i m_i X_i}{\sum_i m_i} \tag{5}$$

where m_i is the mass collected from either the tray or cyclone separator and X_i is the conversion measured at that location via XRD. The mass collected from the cavity was recorded, but not used in the calculation of efficiency or feed rate. The solar input power, $\dot{Q}$, is the nominal power reading of that day's experiment, recorded just before the reactor was placed on sun.

The particle feeding duration (t) is calculated with two methods. The first considers the time between engaging and disengaging the feeding system. The second considers the times when particles start and finish exiting the reactor through the chute, observed using the camera mounted at the air intake of the collection system.

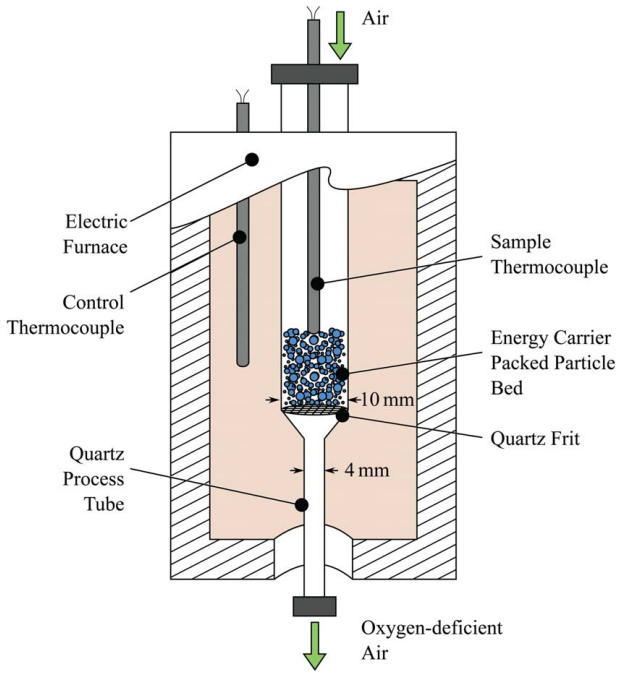

Fig. 2 The benchtop reactor

3.2 Energy Storage. After recovery from the solar reactor's particle collection system, samples of reduced particles were stored in vials in the solar concentrator room of our solar furnace facility. The concentrator room has basic climate control such that its temperature normally fluctuates between 10 and 25 °C. While operating the solar furnace, however, the room is opened to the outdoors. The solar furnace was operated on several occasions during the more than 3-year span of storage, primarily over the summer, such that samples may occasionally have reached temperatures of 30 °C.

3.3 Off-Sun Oxidation Releasing Process Heat. To show the potential of metal oxide redox cycles for on-demand release of stored solar energy as process heat, a sample of the reduced metal oxide was evaluated in an in-house developed benchtop reactor in an experiment conducted on Jan. 13, 2023. As shown in Fig. 2, the benchtop reactor supports an 0.82 g, 10 ± 1 mm long, packed bed of the metal oxide energy carrier particles on a #1 frit, with nominal pore size of 100 − 160 μm, which is fused inside a 10.5 mm ID quartz tube. Downstream of the quartz frit, the inner diameter of the process tube is reduced to 4 mm to minimize dispersion effects.

To facilitate the release of the stored energy through oxidation of the cobalt oxide, a thermal mass flow controller (MKS GE50A Series) delivers compressed air at 194 sccm from top to bottom through the packed bed. A 313 sccm dilution flow of ultra high-purity nitrogen is introduced at the reactor outlet to meet the minimum flow requirements for gas analysis. The oxygen content of the effluent gas is measured by a paramagnetic oxygen analyzer (Siemens Oxymat 6).

The quartz process tube and packed bed are heated in a furnace consisting of two Watlow VS102A12S-A001A heating elements. The furnace temperature is monitored by a control thermocouple and controlled with a PID ramp/soak program run in LABVIEW. The K-type control thermocouple is positioned between the process tube and furnace inner wall. A second K-type thermocouple is located inside the process tube, with its sheath in contact with the top of the packed particle bed. Each thermocouple is fully enclosed by an 0.1875 in diameter alumina sheath.

3.4 Off-Sun Oxidation Producing Hydrogen. To show the potential of hybrid metal oxide redox cycles for on-demand production of hydrogen, a sample of the reduced metal oxide was used on Sep. 28, 2023, in a bulk electrolysis experiment conducted in an electrochemical H-cell (Pine Research Instruments RRPG060) held at room temperature ($T = 22$°C). The H-cell separates the anode and cathode chambers of the cell via a medium frit with a porosity of 10 − 20 μm, preventing the migration of the Co^{2+} reactant to the cathode where it could otherwise be reduced to Co metal

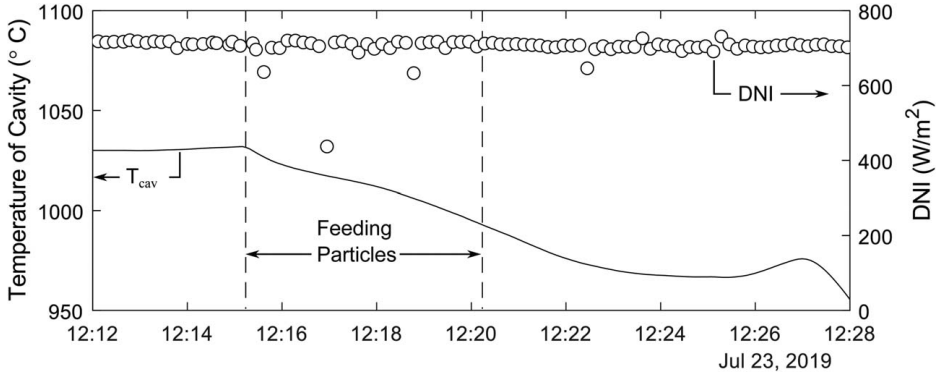

Fig. 3 Cavity temperature (T_{cav}) and DNI during the experiment with the highest mass feed rate of 61 g min^{-1}

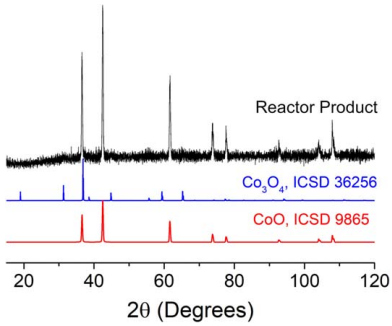

Fig. 4 X-ray diffraction analysis spectra for the sample collected from the cyclone separator jar in the experiment with the highest feed rate of 61 g min^{-1}

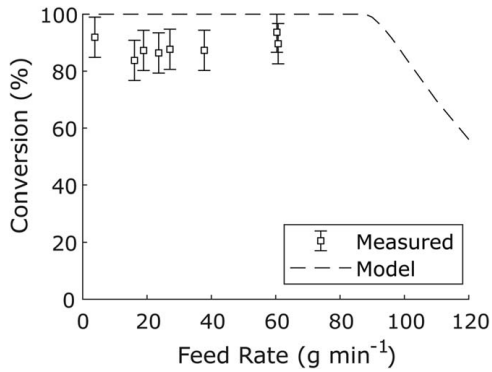

Fig. 5 Variation of mass average Co_3O_4 conversion with feed rate in solar reactor experiments. The feed rate is taken to be the larger of $\dot{m}_{feed}$ and $\dot{m}_{collect}$. Whiskers indicate the uncertainty in conversion measured by X-ray diffraction.

and lower the selectivity[3] of the electrolysis to H_2 [17,18]. The anode chamber included a 21 cm × 13 cm Pt-foil electrode and 20 ml of 45 wt% potassium hydroxide (KOH) with 0.295 g of the reduced metal oxide sample added so that the electrolyte remained saturated with dissolved metal oxide during the experiment. The cathode chamber included a Pt-foil electrode of similar size to the Pt-foil in the anode chamber and 20 ml of 45 wt% KOH without sample added since the metal oxide is not a reactant in the cathodic half-reaction. A Gamry 3000 Potentiostat was used to run bulk electrolysis in a constant potential mode (Chronoamperometry). In this mode, the potentiostat held a constant potential of 0.45 V versus Hg/HgO reference for 90 min. The surface of the resulting Pt anode was characterized with a Renishaw inVia Reflex Raman Spectrometer to confirm the presence of a solid Co^{3+} product. In addition, the current efficiency was estimated as the ratio of the moles of solid product recovered to the moles of electrons (i.e., charge) passed during the bulk electrolysis.

4 Results and Discussion

4.1 On-Sun Solar Reduction. To illustrate the salient features of the on-sun solar reduction experiments, the direct normal irradiance and reactor cavity temperature are shown for the highest feed rate experiment in Fig. 3. The direct normal irradiance remained quite steady near 700 W m^{-2} for the duration of particle feeding. The indicated cavity temperature, measured by a K-type thermocouple positioned between the rotating cavity and the reactor's insulation, reached a maximum temperature of 1032 °C at 12:15 p.m., at which time particle feeding was initiated. Over the duration of particle feeding, the reactor temperature decreases to 993 °C.

After the feed auger is disengaged, the temperature continues to decrease while the particle collection system is still active, reaching a minimum of 967 °C before increasing once the blower is turned off. Finally, the reactor is taken off-sun by closing the solar furnace shutter mechanism and the temperature decreases. This temperature behavior, typical of the full set of reactor experiments, is explained by changes to the reactor energy balance during operation, due to the sensible and chemical energy delivered to the cobalt oxide particles along with the increased convective and advective cooling driven by the particle collection system.

In Fig. 4, we provide the XRD spectrum measured for a sample of particles recovered from the cyclone separator in the experiment with the highest feed rate. This spectrum is typical of all of the spectra obtained for all samples collected from the collection system. For comparison, the XRD spectra of the CoO and Co_3O_4 standards are also provided in the figure. The spectra for the recovered product matches the CoO standard, confirming that the recovered product is predominantly CoO, which is 93% according to Rietveld refinement.

Figure 5 summarizes the conversion of the cobalt oxide particles versus the feed rate. Markers show the conversions attained with the solar rotary drum reactor in the on-sun experiments. Error bars account for the 5% uncertainty at 95% confidence in individual conversion measurements by x-ray diffraction propagated to the mass-averaged conversion. The dashed curve shows the conversion predicted by the model described in the prior work by Kopping et al. [25]. The model predicts complete conversion up to feed rates of 86g min^{-1}, after which the 4 kW solar input is insufficient to supply the chemical energy required for complete conversion while maintaining the target reactor temperature. The feed rates for the reactor experiments, 2.9 to 60.8 g min^{-1}, are within the

[3]Selectivity is also referred to as the current efficiency.

Table 1 Rotary drum reactor on-sun experiments

Date	m_{jar} (g)	X_{jar} (%)	m_{tray} (g)	X_{tray} (%)	$\bar{X}$ (%)	$\dot{Q}_{solar}$ (W)	t_{feed} (min)	$t_{collect}$ (min)	$\dot{m}_{feed}$ (g min^{-1})	$\dot{m}_{collect}$ (g min^{-1})	η_{feed} (%)	c $\eta_{collect}$ (%)
Jul. 11	11.7	76	26.2	99	92	4641	13.0	10.0	2.9	3.8	1	1
Jul. 25	18.7	85	28.0	83	84	3891	6.4	2.9	7.3	16.1	2	5
Jul. 17	83.3	87	30.2	88	87	4310	6.7	6.0	16.8	18.9	5	5
Aug. 2	89.5	96	11.1	75	94	3922	4.6	1.7	21.9	60.4	7	20
Jul. 12	229.0	87	30.9	82	86	4225	11.0	13.0	23.6	20.0	7	6
Jul. 24	156.4	88	26.6	84	88	4098	7.0	6.8	26.1	27.1	8	8
Aug. 7	52.7	87	22.9	88	87	3888	2.0	2.7	37.8	28.3	12	9
Jul. 23	207.1	93	96.7	82	90	3841	5.0	8.1	60.8	37.6	20	12

range predicted to have complete conversion. Experimentally measured conversions do indeed remain high, with a minimum mass weighted average conversion of 84%.

Additional detail for the on-sun solar reduction experiments is provided in Table 1. For each experiment, the table indicates the mass of reduced cobalt oxide collected from the cyclone separator (⑦ in Fig. 1) and the tray at the bottom of the chute (⑤ in Fig. 1), the corresponding particle conversion, mass-averaged conversion, solar power input, duration of particle feeding, feed rate, and the solar-to-chemical energy efficiency for the charging step. The experiments are sorted by the particle feed rate ($\dot{m}_{feed}$). Due to consistently high conversions, the efficiency increases almost proportionally to the feed rate.

We report two values for feed rate and efficiency because they depend on the feeding duration. The two values for the feeding duration correspond to the time for which the auger feeding system was active (t_{feed}) and the duration over which we observed particles entering the collection system with the camera mounted at the air intake ($t_{collect}$). The difference between t_{feed} and $t_{collect}$ is an artifact of short feeding lengths, chosen primarily not only to limit the total mass of cobalt used in the experimental program but also to facilitate a relatively steady solar input for the duration of feeding, as shown in Fig. 3. The durations differ because of accumulation of particles in the cavity. After activating the auger, particles accumulate in the cavity for a period of time before we observe them entering the collection system. This time is more significant at lower feed rates, which is why $t_{collect} < t_{feed}$ at lower feed rates. After deactivating the auger, particles accumulated in the cavity continue to enter the collection system, though some particles remain in the cavity at the end of the experiment. This second effect is more significant at higher feed rates. In the two highest feed rate experiments, we observed a marked decrease in the rate of particles entering the collection system after deactivating the auger. A video recording showing the particles exiting the reactor during the highest feed rate experiment, conducted on July 23, is available through *ValpoScholar* [29]. Because most of the mass appears to have been recovered over the shorter duration, t_{feed}, $\dot{m}_{feed}$, and η_{feed} seem to provide the better description of the experimental findings at higher feed rates.

We include only the reduced cobalt collected in the particle collection system, i.e., m_{tray} and m_{jar}, in the feed rate calculations. Particles collected from the reactor cavity are not included in the reported feed rates, mass average conversions, or efficiencies because they did not successfully exit the reactor system. At the end of most experiments, we did collect measurable masses of particles from the cavity. These particles had much lower conversion, near 10–15%, according to XRD analysis. The lower conversion of particles collected from the cavity is attributed to much slower cooling while exposed to air, relative to the particles that entered the collection system.

The mass weighted average conversions exceed those achieved in prior on-sun reduction of cobalt oxide particles by Neises et al. [1] and Palumbo et al. [26]. To our knowledge, they represent the highest conversion for cobalt oxide reduced in a solar reactor. While high, the measured conversions indicate that the recovered

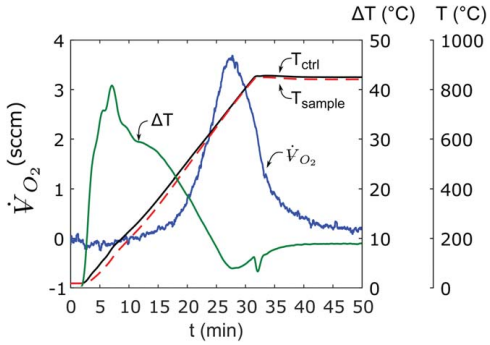

Fig. 6 Rate of oxygen uptake ($\dot{V}_{O_2}$) during heating of the cobalt oxide previously reduced on-sun on July 23 (see Table 1). Also shown are the indicated sample temperature (T_{sample}), furnace control temperature (T_{ctrl}), and the difference between the two temperatures (ΔT).

particles still contain a lesser fraction of Co_3O_4. As a possible explanation, we surmise that the particles were fully reduced in the reactor cavity and subsequently were partially oxidized as they cooled in the presence of air in our particle extraction system. Even so, the measured conversions show great potential for a rotating drum reactor like the one tested to enact continuous reduction of metal oxide particles.

Of practical interest, the reactor facilitated many additional experiments spanning more than a year prior to those presented here. A series of 13 experiments are described by Palumbo et al. [26]. After those experiments, the feed system was redesigned to enable higher feed rates. Seven additional on-sun experiments were run in 2019 as we worked to refine the particle feed system in its final version. Including the experiments presented here, the reactor was subjected to at least 28 cycles of heating to approximately 1000 °C and subsequent cooling to room temperature. From a thermo-mechanical design standpoint, the reactor was found to be quite robust, with occasional repainting of the aperture cone with zirconia paste as the only required maintenance.

4.2 Off-Sun Oxidation Releasing Process Heat. Nearly 3.5 years after concentrated sunlight drove the reduction of the particles, a sample of the reduced cobalt oxide particles from the highest feed rate solar reactor experiment (July 23) was selected to demonstrate the release of the stored solar energy as process heat via the reaction in Eq. (2). As described in Sec. 3.3, the sample was heated in a quartz process tube under a constant flow of zero air. The experiment demonstrates the release of the stored solar energy by quantifying the rate of the oxidation of the cobalt particles through measurement of the oxygen uptake. The volumetric rate of oxygen uptake ($\dot{V}_{O_2}$) is shown along with the temperatures indicated by the furnace control (T_{ctrl}) and sample thermocouples (T_{sample}) and the difference between the two temperatures (ΔT) in Fig. 6. The rate of oxygen uptake increases during

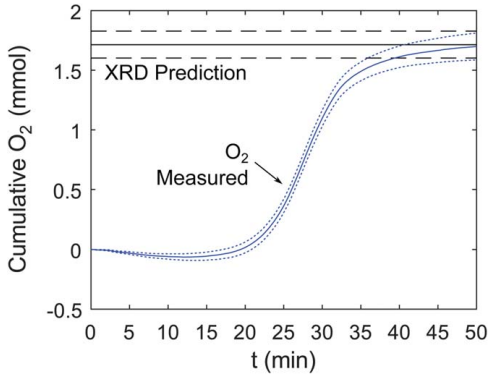

Fig. 7 Cumulative molar oxygen uptake by the reduced cobalt oxide based on the rate of oxygen uptake in Fig. 6 compared to available oxygen capacity predicted by X-ray diffraction of solar-reduced Co_3O_4

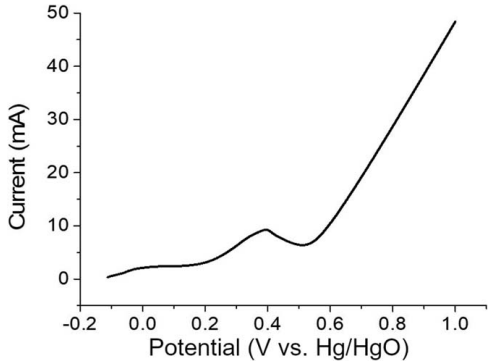

Fig. 8 Linear sweep voltammogram obtained in the electrochemical H-cell at a scan rate of 100 m$V\,s^{-1}$. The potential at the anode is relative to a Hg/HgO reference.

heating until it reaches a maximum of 3.5 sccm at a sample temperature of 734 °C. Subsequently, the rate of oxygen uptake declines as the sample temperature increases to a maximum of 851 °C and plateaus at 841 °C.

During heating, the sample temperature lags behind the control temperature. The difference between the two temperatures decreases as the setpoint temperature of 850 °C is approached. In part, the shrinking difference between temperatures can be explained by improved radiative heat transfer as the furnace temperature increases. However, the difference between temperatures indicated by the control and sample thermocouples reaches a minimum of 4 °C, just as the rate of oxygen uptake by the previously reduced cobalt oxide reaches its maximum, which occurs *before* the furnace control temperature reaches the 850 °C setpoint. As the furnace continues heating, the temperature difference then increases before stabilizing at 9 °C as the reaction reaches completion. Both the concurrence of the minimum ΔT with the maximum reaction rate and the subsequent increase in ΔT during further heating are explained by the release of the stored solar energy through the exothermic oxidation of CoO, Eq. (2).

The cumulative oxygen consumed by the reaction is shown in Fig. 7. For comparison, the oxygen capacity of the sample based on x-ray diffraction measurements of conversion from the on-sun reactor experiment is also shown. Upper and lower bounds on the capacity account for uncertainty in the conversion measurement from the on-sun experiment and measurement of the sample mass for the off-sun experiment. Bounds on the measured oxygen consumption represent an engineering estimate of uncertainty at 95% confidence in the measurement of oxygen release, including contributions from the mass flowrate and oxygen concentration

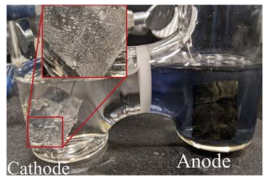

Fig. 9 Photograph of the H-cell during bulk electrolysis depicting the H_2 gas bubbles on the cathode the surface (inset) and the solid black deposit on the anode

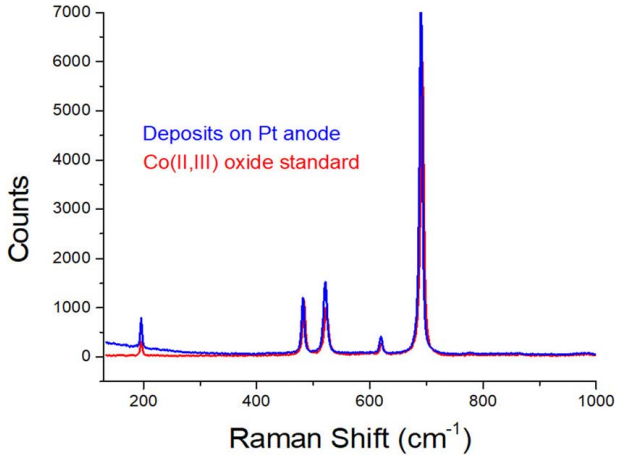

Fig. 10 Raman spectrograph of the black deposit collected from the anode

measurements. The measured oxygen consumption falls within the predicted bounds for the oxygen capacity. This result not only suggests that the reduced cobalt oxide was chemically stable for the more than 3 years of storage but also that it retained complete capacity to release the stored solar energy.

4.3 Off-Sun Oxidation Producing Hydrogen. A second sample of the solar-reduced cobalt oxide particles from the highest feed rate experiment was used to demonstrate solar production of H_2 via solar thermal decoupled electrolysis, Eq. (3). The sample was dissolved in the 45 wt% KOH electrolyte on the anodic side of the electrochemical H-cell as described in Sec. 3.4, and linear sweep voltammetry (LSV) and bulk electrolysis experiments were performed. The experiments demonstrate the production of H_2 and confirm that the chemical potential of the reduced cobalt oxide lowers the electrical potential required to produce H_2 below that required for direct splitting of H_2O, as first shown by Nudehi et al. [17]. The experiment further demonstrates that the solid product of the process can be recovered to complete the redox cycle.

As shown in the linear sweep voltammogram of Fig. 8, an oxidation reaction proceeds on the anode at +0.45 V (versus Hg/HgO) near the local maxima in current at +0.40 V. A 0.45 V potential versus Hg/HgO corresponds to a cell potential of about 0.55 V versus NHE, approximately half the 1.23 V thermodynamic equilibrium potential when O_2(g) first begins to evolve at the anode. The LSV thus suggests that the oxidation reaction at the anode is the oxidation of the dissolved CoO from the sample (Eq. (3)).

Consequently, we performed a chronoamperometry experiment over 90 min at a constant potential of +0.45 V versus Hg/HgO to look for the production of H_2 at the cathode and a solid Cobalt(II, III) product on the anode. During the experiment, we observed gas bubbles forming on the surface of the cathode alongside deposition of a black solid on the anode, as depicted in Fig. 9. There was no evidence of gas formation on the anode. The most probable gaseous product to form at the cathode in the presence of the

KOH solution is H_2 via the hydrogen evolution half-reaction, Eq. (6).

$$2H_2O + 2e^- \rightarrow H_2(g) + 2OH^- \quad (6)$$

where the electrons in Eq. (6) are supplied to the cathode through the potentiostat via the CoO-oxidation half-reaction at the anode, Eq. (7).

$$3CoO + 2OH^- \rightarrow Co_3O_4 + 2e^- + H_2O \quad (7)$$

The net effect of half-reactions (6) and (7) is the oxidation of CoO by H_2O to produce H_2 and Co_3O_4. The presence of gas bubbles on the cathode, the absence of gas bubbles on the anode, and the observation of a solid deposition on the anode provide strong evidence for the production of H_2 via Eq. (3).

To further confirm that the oxidation of the reduced cobalt oxide drove the production of H_2 in the electrolysis experiment, we collected and analyzed the solid black product that formed on the anode by Raman spectroscopy with 532 nm excitation. The black substance produced an identical Raman spectrum to a Cobalt(II, III) oxide standard (Fig. 10). The anode mass decreased by 1.14 mg after the black cobalt oxide deposit was cleaned from its surface, indicating a current efficiency of 88%, similar to what was reported previously [17]. When the Raman result and the measured current efficiency are combined with physical observation of the H-cell during the electrolysis and the LSV, the results overwhelmingly suggest that H_2 was produced in the electrolysis experiment by solar thermal decoupled electrolysis using a CoO reactant produced on-sun nearly 3.5 years prior.

5 Conclusion

As predicted by Kopping et al. [25], maintaining a temperature above 960 °C enabled consistent, high conversion of Co_3O_4 to CoO. We measured conversions of 84–94% for the set of eight on-sun experiments with the prototype solar rotary drum reactor for feed rates between 2.9 and 60.8 g min^{-1}.

After storage for more than 3 years, the particles were heated under exposure to air to demonstrate the capacity of the thermochemical energy storage approach to dispatch energy as needed. Within measurement uncertainty, the reduced cobalt oxide completely retained its capacity to release the stored thermochemical energy.

In addition, the particles were dissolved in the basic electrolyte (KOH) of an aqueous electrochemical cell and electrochemically oxidized in bulk electrolysis to demonstrate dispatchable production of H_2. Hydrogen production was verified visually with the application of a potential of about 0.55 V. This potential is 0.68 V less than the thermodynamic equilibrium potential required for the direct splitting of H_2 O in a base (1.23 V), validating that the energy stored in the solar-produced CoO was transferred to the H_2 fuel. Importantly, the solid metal oxide product of the process was recovered and shown to contain Co(II,III) oxide to close the redox cycle.

The demonstrated performance of cobalt oxide as a multiyear, fungible solar energy storage medium warrants further consideration. The ability to dispatch the storage for process heat or fuel production offers energy project developers access to two energy markets, flexibility that could enhance project revenues over alternative long duration storage options. Future efforts should evaluate the economics of cobalt oxide as an energy carrier, the capacity of the cobalt oxide particles to withstand repeated cycling, methods to ensure that particles are completely retained within the system, and approaches to increase the current density of the electrochemical oxidation of the particles for H_2 production.

Acknowledgment

We thank Rich Diver and Bob Palumbo for input on early reactor concepts and the 2015–2016, 2016–2017, and 2017–2018 Valparaiso University Senior Design teams for their work on multiple iterations to design and realize the solar rotary drum reactor. Undergraduate research student Alex Kagay was instrumental in configuring the benchtop reactor and its auxiliary equipment. Purchase of the Raman microscope used to obtain results included in this publication was supported by the National Science Foundation under the award CHE MRI 2215322.

Funding Data

- U.S. National Science Foundation (CHE MRI Award No. 2215322).
- U.S. National Science Foundation (RUI Award No. 1334896).
- U.S. Indiana Space Grant Consortium (INSGC) (Subaward No. 12000338-337).

Conflict of Interest

There are no conflicts of interest.

Data Availability Statement

The datasets generated and supporting the findings of this article are obtainable from the corresponding author upon reasonable request.

Nomenclature

k = thermal conductivity (W m^{-1} K^{-1})
m = solid mass (g)
t = particle feeding duration (min)
$\dot{m}$ = mass feed rate (g min^{-1})
X = conversion of Co_3O_4 to CoO (–)
$\dot{V}$ = volumetric gas flowrate (sccm)
$\dot{Q}_{solar}$ = solar input power (W)

Greek Symbols

ΔH_r = enthalpy of reaction (kJ kg^{-1})
η = reactor efficiency (–)

Abbreviations

DNI = direct normal irradiance
NHE = normal hydrogen electrode

References

[1] Neises, M., Tescari, S., de Oliveira, L., Roeb, M., Sattler, C., and Wong, B., 2012, "Solar-Heated Rotary Kiln for Thermochemical Energy Storage," Sol. Energy., **86**(10), pp. 3040–3048.
[2] Agrafiotis, C., Pein, M., Giasafaki, D., Tescari, S., Roeb, M., and Sattler, C., 2019, "Redox Oxides-Based Solar Thermochemistry and Its Materialization to Reactor/Heat Exchanger Concepts for Efficient Solar Energy Harvesting, Transformation and Storage," ASME J. Sol. Energy. Eng., **141**(2), p. 021010.
[3] Jackson, G. S., Imponenti, L., Albrecht, K. J., Miller, D. C., and Braun, R. J., 2019, "Inert and Reactive Oxide Particles for High-Temperature Thermal Energy Capture and Storage for Concentrating Solar Power," ASME J. Sol. Energy. Eng., **141**(2), p. 021016.
[4] Buck, R., Agrafiotis, C., Tescari, S., Neumann, N., and Schmücker, M., 2021, "Techno-Economic Analysis of Candidate Oxide Materials for Thermochemical Storage in Concentrating Solar Power Systems," Front. Energy Res., **9**, pp. 1–13.

[5] Palumbo, R., Diver, R. B., Larson, C., Coker, E. N., Miller, J. E., Guertin, J., Schoer, J., Meyer, M., and Siegel, N. P., 2012, "Solar Thermal Decoupled Water Electrolysis Process I: Proof of Concept," Chem. Eng. Sci., **84**, pp. 372–380.
[6] Tescari, S., Agrafiotis, C., Breuer, S., de Oliveira, L., Puttkamer, M. N.-v., Roeb, M., and Sattler, C., 2014, "Thermochemical Solar Energy Storage via Redox Oxides: Materials and Reactor/Heat Exchanger Concepts," Energy Procedia, **49**, pp. 1034–1043.
[7] Singh, A., Tescari, S., Lantin, G., Agrafiotis, C., Roeb, M., and Sattler, C., 2017, "Solar Thermochemical Heat Storage via the Co_3O_4/CoO Looping Cycle: Storage Reactor Modelling and Experimental Validation," Sol. Energy., **144**, pp. 453–465.
[8] Agrafiotis, C., Tescari, S., Roeb, M., Schmücker, M., and Sattler, C., 2015, "Exploitation of Thermochemical Cycles Based on Solid Oxide Redox Systems for Thermochemical Storage of Solar Heat. Part 3: Cobalt Oxide Monolithic Porous Structures as Integrated Thermochemical Reactors/Heat Exchangers," Sol. Energy., **114**, pp. 459–475.
[9] Tescari, S., Singh, A., Agrafiotis, C., de Oliveira, L., Breuer, S., Schlögl-Knothe, B., Roeb, M., and Sattler, C., 2017, "Experimental Evaluation of a Pilot-Scale Thermochemical Storage System for a Concentrated Solar Power Plant," Appl. Energy., **189**, pp. 66–75.
[10] Schrader, A. J., Muroyama, A. P., and Loutzenhiser, P. G., 2015, "Solar Electricity via an Air Brayton Cycle With an Integrated Two-Step Thermochemical Cycle for Heat Storage Based on Co3O4/CoO Redox Reactions: Thermodynamic Analysis," Sol. Energy., **118**, pp. 485–495.
[11] Schrader, A. J., De Dominicis, G., Schieber, G. L., and Loutzenhiser, P. G., 2017, "Solar Electricity via an Air Brayton Cycle With an Integrated Two-Step Thermochemical Cycle for Heat Storage Based on Co3O4/CoO Redox Reactions III: Solar Thermochemical Reactor Design and Modeling," Sol. Energy., **150**, pp. 584–595.
[12] Karagiannakis, G., Pagkoura, C., Halevas, E., Baltzopoulou, P., and Konstandopoulos, A. G., 2016, "Cobalt/Cobaltous Oxide Based Honeycombs for Thermochemical Heat Storage in Future Concentrated Solar Power Installations: Multi-Cyclic Assessment and Semi-quantitative Heat Effects Estimations," Sol. Energy., **133**, pp. 394–407.
[13] Zhou, X., Mahmood, M., Chen, J., Yang, T., Xiao, G., and Ferrari, M. L., 2019, "Validated Model of Thermochemical Energy Storage Based on Cobalt Oxides," Appl. Therm. Eng., **159**, p. 113965.
[14] Turchi, C. S., Ma, Z., Neises, T. W., and Wagner, M. J., 2013, "Thermodynamic Study of Advanced Supercritical Carbon Dioxide Power Cycles for Concentrating Solar Power Systems," ASME J. Solar Energy Eng., **135**(4), p. 041007.
[15] Crespi, F., Gavagnin, G., Sánchez, D., and Martínez, G. S., 2017, "Supercritical Carbon Dioxide Cycles for Power Generation: A Review," Appl. Energy., **195**, pp. 152–183.
[16] Agrafiotis, C., Roeb, M., and Sattler, C., 2014, "Cobalt Oxide-Based Structured Thermochemical Reactors/Heat Exchangers for Solar Thermal Energy Storage in Concentrated Solar Power Plants," Proceedings of the ASME 8th International Conference on Energy Sustainability, American Society of Mechanical Engineers, p. V001T02A005.
[17] Nudehi, S., Larson, C., Prusinski, W., Kotfer, D., Otto, J., Beyers, E., Schoer, J., and Palumbo, R., 2018, "Solar Thermal Decoupled Water Electrolysis Process II: An Extended Investigation of the Anodic Electrochemical Reaction," Chem. Eng. Sci., **181**, pp. 159–172.
[18] Silcox, R., Engerer, L. K., Nudehi, S., Smith, P., Schoer, J., Krenzke, P. T., Palumbo, R., and Venstrom, L. J., 2020, "Solar Thermal Decoupled Water Electrolysis Process III: The Anodic Electrochemical Reaction in a Rotating Disc Electrode Cell," Chem. Eng. Sci., **227**, p. 115885.
[19] Mills, B. H., Ho, C. K., Schroeder, N. R., Shaeffer, R., Laubscher, H. F., and Albrecht, K. J., 2022, "Design Evaluation of a Next-Generation High-Temperature Particle Receiver for Concentrating Solar Thermal Applications," Energies, **15**(5), p. 1657.
[20] Moumin, G., Tescari, S., Sundarraj, P., de Oliveira, L., Roeb, M., and Sattler, C., 2019, "Solar Treatment of Cohesive Particles in a Directly Irradiated Rotary Kiln," Sol. Energy., **182**, pp. 480–490.
[21] Tescari, S., Moumin, G., Bulfin, B., De Oliveira, L., Schaefer, S., Overbeck, N., Willsch, C., Spenke, C., Thelen, M., Roeb, M., and Sattler, C., 2018, "Experimental and Numerical Analysis of a Solar Rotary Kiln for Continuous Treatment of Particle Material," AIP. Conf. Proc., **2033**, pp. 1–8.
[22] Müller, R., Haeberling, P., and Palumbo, R. D., 2006, "Further Advances Toward the Development of a Direct Heating Solar Thermal Chemical Reactor for the Thermal Dissociation of ZnO(s)," Sol. Energy., **80**(5), pp. 500–511.
[23] Ebert, M., Amsbeck, L., Buck, R., Rheinländer, J., Schlögl-Knothe, B., Schmitz, S., Sibum, M., Stadler, H., and Uhlig, R., 2018, "First On-Sun Tests of a Centrifugal Particle Receiver System," ASME 2018 12th International Conference on Energy Sustainability Collocated with the ASME 2018 Power Conference and the ASME 2018 Nuclear Forum, Lake Buena Vista, FL, June 24–28, p. V001T11A002.
[24] Ebert, M., Amsbeck, L., Rheinländer, J., Schlögl-Knothe, B., Schmitz, S., Sibum, M., Uhlig, R., and Buck, R., 2019, "Operational Experience of a Centrifugal Particle Receiver Prototype," AIP. Conf. Proc., **2126**(1), p. 030018.
[25] Kopping, S. J., Hoeniges, J., Greenhagen, J., Matejczyk, Z., and Venstrom, L. J., 2019, "Model of the Solar-Driven Reduction of Cobalt Oxide in a Particle Suspension Reactor," Sol. Energy., **177**, pp. 713–723.
[26] Palumbo, R., Venstrom, L. J., and Nudehi, S., 2022, "High-Temperature Solar Thermal Electrochemistry With Metal Oxides," Handbook of Solar Thermal Technologies, World Scientific, Singapore, pp. 173–228.
[27] Duncan, G. S., Nudehi, S., Palumbo, R., and Venstrom, L. J., 2014, "A High-Flux Solar Furnace for Undergraduate Engineering Education and High-Temperature Thermochemistry Research," Proceedings of the ASME 8th International Conference on Energy Sustainability, Vol. 1, pp. 1–7.
[28] Lipinski, W., Davidson, J. H., Haussener, S., Klausner, J. F., Mehdizadeh, A. M., Petrasch, J., Steinfeld, A., and Venstrom, L., 2013, "Review of Heat Transfer Research for Solar Thermochemical Applications," ASME J. Therm. Sci. Eng. Appl., **5**(2), p. 021005.
[29] Krenzke, P. T., 2023, "Demonstration of Multiyear Solar Thermochemical Energy Storage via the Cobalt Oxide Cycle," ValpoScholar: Engineering Faculty Publications, Patents, Presentations, Video, 10:23, https://scholar.valpo.edu/engineering_fac_pub/123.